Marine Geology 252 (2008) 24–37

Contents lists available at ScienceDirect

Marine Geology

journal homepage: www.elsevier.com/locate/margeo

Episodic dynamics of a sand wave field

Shelley J. Whitmeyer *, Duncan M. FitzGerald

Department of Earth Sciences, Boston University, 675 Commonwealth Ave, Boston, MA 02215 USA

ARTICLE INFO

Article history:
Received 24 March 2007
Received in revised form 6 March 2008
Accepted 20 March 2008

Keywords:
sand wave
Moriches Inlet
episodic dynamics
inlet
bedform

ABSTRACT

The morphodynamics of a sand wave field in a flood-dominant channel inside Moriches Inlet was monitored for eight weeks during the summer of 2005. Bathymetric data show sand waves on average are 15 m long and 39 cm high with shallow slip faces. The sand waves remained stationary over the eight-week study. The maximum peak current speeds recorded during this study only reached 60 cm/s. This velocity was not sufficient to cause measurable sand wave migration. Analysis based on work by van Rijn suggests that the sand waves of this size would be created when the current velocity exceeds 80 cm/s, conditions not observed during this study.

Water level data from Sandy Hook, NJ, and Shinnecock Inlet, NY, show that large tidal ranges occur when a drop in barometric pressure increases the elevation of high tide and strong north winds decrease the low-tide elevation. During these events the current velocity may reach 80 cm/s, which is predicted to be strong enough to produce these sand waves. This study demonstrates that high-energy, episodic events may control sand wave morphology at Moriches Inlet.

1. Introduction

Bedforms of various scales are prevalent in most aqueous environments (Ashley, 1990; Soulsby, 1997; Hulscher and Dohmen-Janssen, 2005). They affect seabed roughness and flow conditions and, therefore, sediment transport (Engelund and Fredsoe, 1982). In addition, the presence and migration of large bedforms may create navigation hazards (Aliotta and Perillo, 1987; Lillycrop et al., 1989; Granat and Alexander, 1991; Levin et al., 1992; Katoh et al., 1998; Johnston et al., 2002; Knaapen and Hulscher, 2002; Redding, 2002; Hulscher and Dohmen-Janssen, 2005), undermine submarine pipelines (Morelissen et al., 2003), or block intake valves. Understanding the morphology and dynamics of sand waves will help mitigate these potential hazards and improve our understanding of sediment transport.

Substantial progress has been made in the understanding of the physical factors controlling the development of sand waves, which may also be referred to as medium to large dunes (Ashley, 1990). Sand wave geometry has been related to water depth (Yalin, 1964; van Rijn, 1984b; Aliotta and Perillo, 1987; Dalrymple and Rhodes, 1995; Carling et al., 2000; Li and King, 2007), grain size (McCave, 1971; Southard, 1971; Bokuniewicz et al., 1977; Rubin and McCulloch, 1980; Zarillo, 1982; Dalrymple, 1984; Aliotta and Perillo, 1987; Southard and Boguchwal, 1990b; Dalrymple and Rhodes, 1995; Bartholdy et al., 2002; Ernstsen et al., 2005), and current velocity (Simons and Richardson, 1961; Boothroyd and Hubbard, 1974; Zarillo, 1982; Dalrymple, 1984; van Rijn, 1984b; Ashley, 1990; Dalrymple and Rhodes, 1995). Yalin (1964), Engelund and Fredsoe (1982), Allen (1980), and van Rijn (1984b) are just a few of the researchers who have used these parameters to predict the morphology of the seabed. However, in natural systems simple, one-to-one relationships between these parameters and sand wave morphology are not always observed because the morphology and hydraulic conditions may not be in equilibrium. Instead the morphology maybe controlled by the availability of sediment (i.e. thickness of surficial sediment) (Aliotta and Perillo, 1987; Dalrymple and Rhodes, 1995; Carling et al., 2000; Hoekstra et al., 2004), antecedent morphology, or prior flow conditions.

Presented here is a detailed hydraulic and morphologic study of a sand wave field in Moriches Inlet, Long Island, New York, USA (Fig. 1). The findings are based on bathymetric, hydrodynamic, and grain size data collected over a 2 yr span and include eight weekly bathymetric surveys of the study region. This study is unique in the detail and frequency of the surveys. The results show that the sand wave morphology in Moriches Inlet, NY, USA, is controlled by episodic storm events, not mean flow conditions. This finding suggests that the extreme, low-frequency, high-energy, events may be as important as the mean flow conditions when describing sand waves.

2. Regional setting

The backbone of Long Island is composed of the Ronkonkoma Moraine and the Harbor Hill Moraine deposited by the Laurentide Ice

* Corresponding author. Present Address: MSC 6903, Memorial Hall, James Madison University, Harrisonburg, VA 22807, USA. Tel.: +1 540 421 3420; fax: +1 540 568 8058.
E-mail address: whitm2sj@jmu.edu (S.J. Whitmeyer).

0025-3227/$ – see front matter © 2008 Elsevier B.V. All rights reserved.
doi:10.1016/j.margeo.2008.03.009

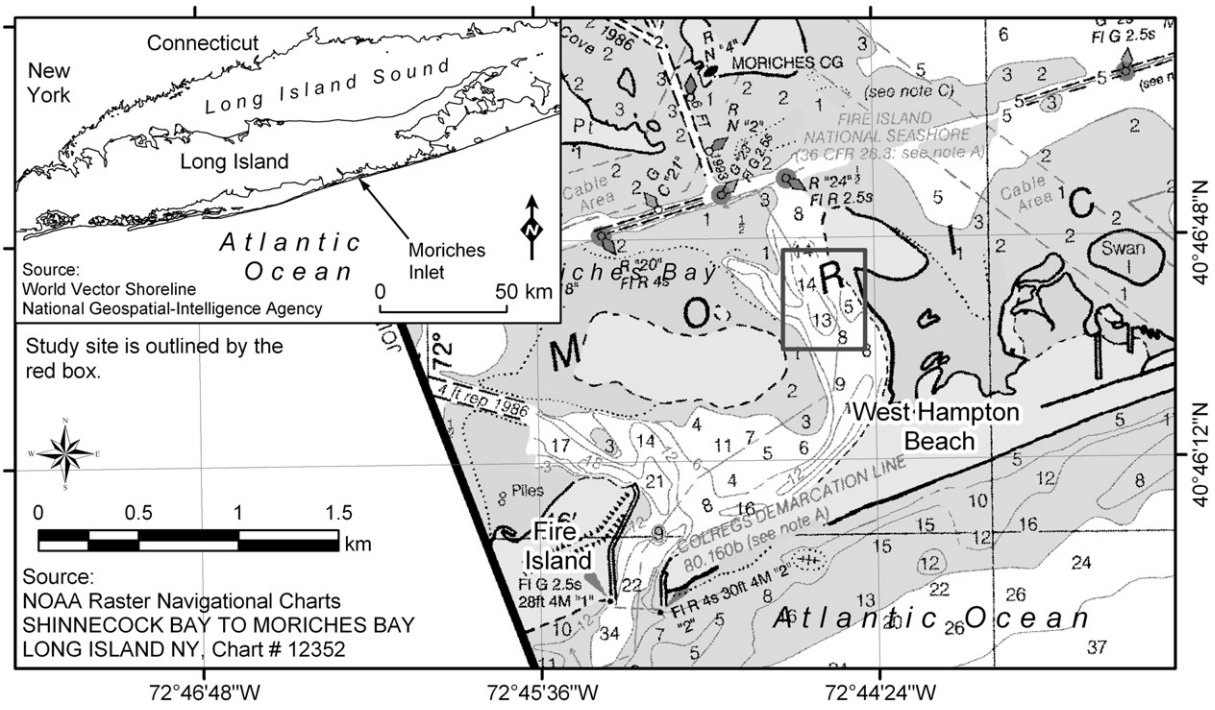

Fig. 1. Location of the study area within Moriches Bay. Study site is delineated by the box.

Sheet 18,000 yr ago (Sirkin, 1995). Reworking of the sandy outwash plain sediment south of the Ronkonkoma Moraine has led to the development of a barrier island chain along the southern shoreline. Moriches Inlet, one of six semi-permanent inlets along this stretch of coast, is located 100 km east of New York City and 80 km west of Montauk Point. It connects Moriches Bay to the Atlantic Ocean. Moriches Inlet formed in 1931 when the barrier was breached by a major storm.

Moriches Bay is a shallow, elongate lagoon, 18 km long (east–west) and less than 4 km wide at its widest point. Forty percent of the bay is shallower than 1 m mllw, and more than 90% is shallower than 2 m mllw. There is no significant input of fresh water to the bay.

Moriches Bay is microtidal with a mean tidal range at the inlet of 0.9 m, and a spring tidal range of 1.07 m.[1] At the Coast Guard Station on the northern shore of Moriches Bay, about 0.5 km north of the study area, the spring/mean tidal range is 0.77/0.66 m. At the study site the spring range is 1.0 m, and the neap range is 0.6 m.

The focus of this study is a sand wave field in the eastern flood channel (2–4 m deep) inside Moriches Inlet. The sand wave field is located on a shallow bank (~2–3 m deep) between two tidal channels (~4 m deep); on the west is an ebb-dominant channel and to the east is a flood-dominant channel. Sand waves on the bank are flood-oriented and better-defined than those on the ebb channel. The sand waves in the ebb channel are ebb-oriented and smaller than those on the sand bank. These sand waves are persistent features in this area and have been documented on aerial photographs from 2001 and 2004 as well as bathymetric surveys from June 2004 and July/August 2005. Because this portion of the bay is shallow and the fetch is limited, this region is dominated by tidal currents. Wave height/period estimates based on fetch and wind velocity predict wave heights to be <~0.5 m and the period to be 2.1 s (Shore Protection Manual, 1984), even during large storm events where wind speeds may reach 20 m/s. These conditions would produce near bottom velocity of about 0.22 m/s, which does not exceed the critical velocity for the initiation of sediment transport at the study area.

3. Data and methods

This study integrates bathymetric, hydraulic, and sedimentological data to provide a comprehensive description of a sand wave field in Moriches Bay. This site was chosen because it is a low-energy environment which is still able to support sand waves. In addition, the area is sand rich which minimizes the reduction of sand wave size due to limited sediment supply. Data were collected over eight weeks during the summer of 2005, with the exception of the sediment samples that were collected the previous summer. The sampling period covered four neap spring cycles and surveys were performed during various tide stages depending on the week.

3.1. Bathymetry

Weekly bathymetric surveys were collected with an Innerspace Model 455 single-beam depth sounder (200 kHz and 8°). The location of the boat was tracked with a Trimble AgGPS 132 GPS (sub-meter accuracy). Two surveys were taken over the first 24 h to capture sand wave response to a spring tide (Table 1). Thereafter, the surveys were conducted weekly (29 July, 5 August, 12 August, 19 August, 26 August,

Table 1
Survey index

Date	Tide	Tide range (m)
21 July 2005	Ebb	1.0
22 July 2005	Ebb	0.93
29 July 2005	Flood	0.66
5 August 2005	Ebb	0.67
12 August 2005	Flood	0.63
19 August 2005	Ebb	0.90
26 August 2005	Flood	0.71
2 September 2005	Ebb	0.61

[1] Tidal ranges for Moriches Inlet and Coast Guard Station were downloaded from the NOAA/NOS Tidal Station Locations and Ranges web page, http://140.90.121.76/tides06/tab2ec2a.html, on April 26, 2006.

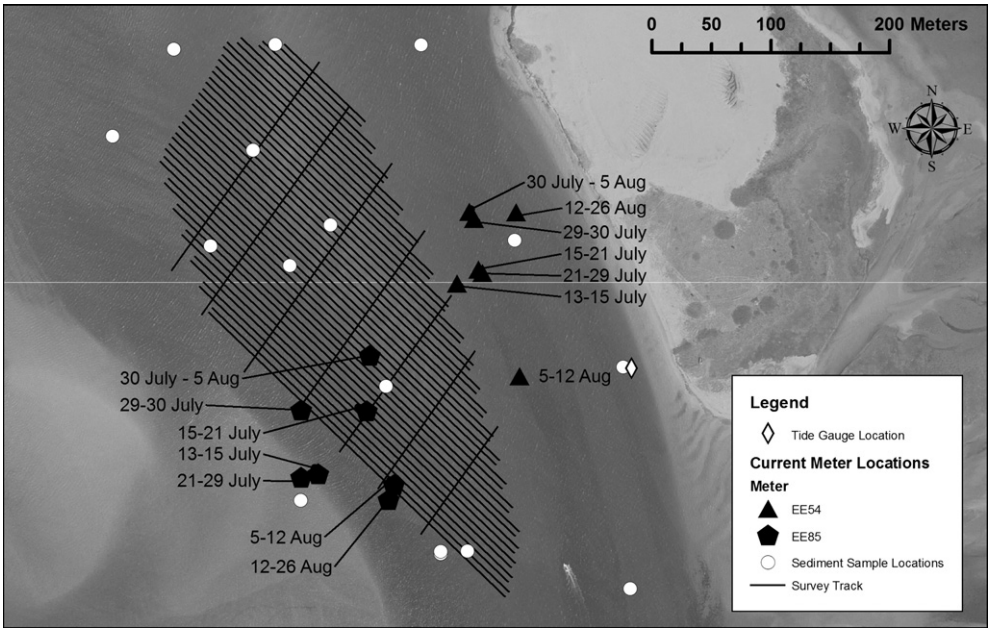

Fig. 2. Field map.

and 2 September). During each survey, soundings were collected along 40 transects that ran along the channel, perpendicular to the sand wave crests (northwest – southeast). These transects were spaced about 5 m apart (Fig. 2). Seven additional transects were run across the channel (southwest–northeast) to better constrain the cross section of the channel and provide data to perform a cross-line accuracy check. The cross-channel lines were run approximately 3 h after the first along channel lines. There was no noticeable offset between the along and across channel transects. To minimize errors, the depth sensor was calibrated throughout the surveys with a bar check, and surveys were collected early in the morning when wave disturbance was minimal. The soundings were post-processed to remove the tidal signal. Water level data from the tide gauge were used to correct the soundings for the tide stage. During post-processing, any obvious spikes caused by turbulence in the water column or boat wakes were removed.

Bathymetric surfaces were modeled with ArcGIS™. A Triangulated Irregular Network (TIN) was created from the individual soundings for each survey. The TINs were converted to grids in order to run more efficiently in ArcMap™ (Fig. 3). To test the error associated with the interpolation process, the surfaces were recreated using data from only half of the transects. The interpolation error was estimated from the differences between the modeled surface and the elevation of the data points not used in the interpolation. The mean error was ±12 cm.

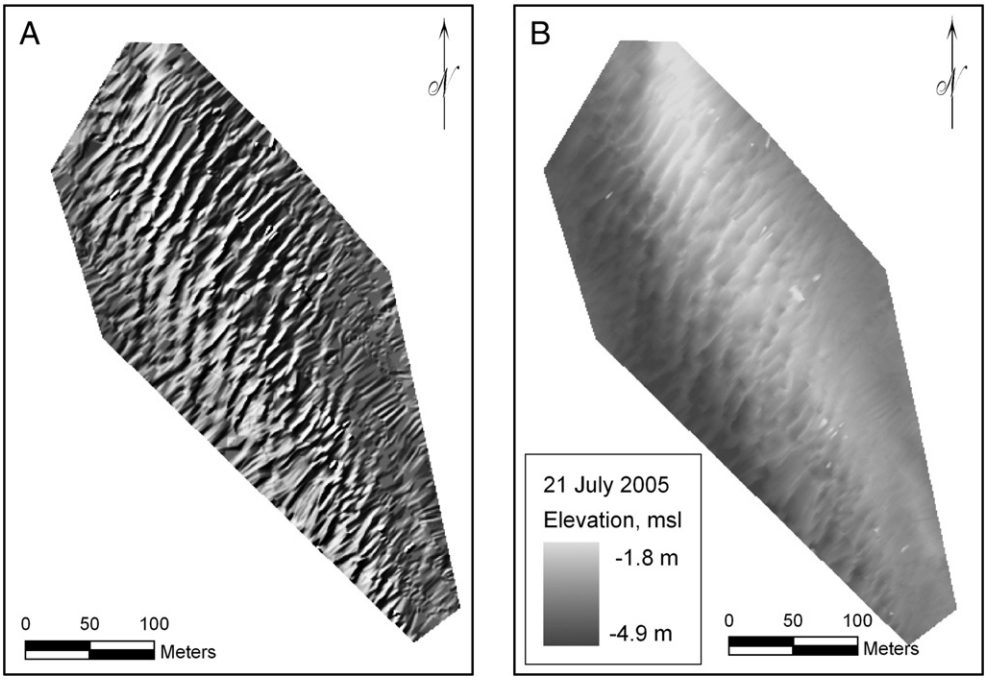

Fig. 3. A) Hillshade map rendered from bathymetry collected on 21 July 2005. The sand waves are clearly defined on the hillshade map. B) Bathymetric map of the study area on 21 July 2005. The map is a 1-m grid.

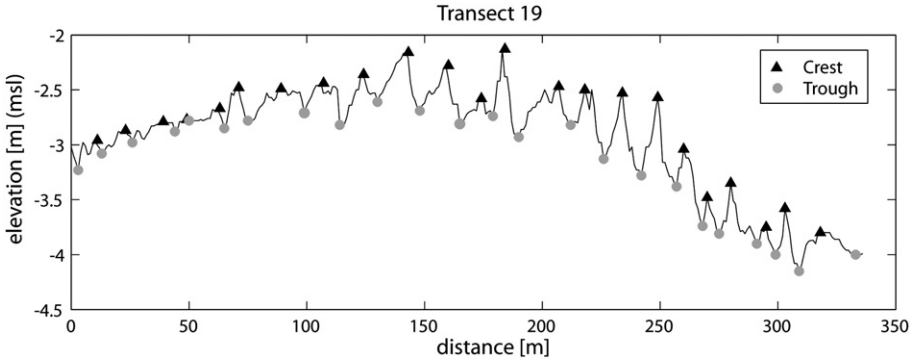

Fig. 4. Cross section from transect 19 which runs through the center of the study area. Crests are shown as triangles, and the troughs are shown as circles.

This error is conservative, as the resolution was only half of the original survey. Higher resolution data will result in a smaller interpolation error. The interpolation error best describes the uncertainty of the bathymetric data because it is larger than any of the errors expected to occur during data collection and all of the sources of error are independent of one another.

The sand wave location, height, wavelength, and orientation were identified on each of the eight surveys. This analysis was semi-automated, using both plan view bathymetric maps and cross sections. Cross-sectional profiles were extracted from the bathymetric grid along each of the survey lines running northwest–southeast and then imported into MatLab® for analysis with a script written by the author. The crests and troughs of the sand waves were identified by calculating the approximate derivative of each cross section (Fig. 4). The wavelength, height, and slope of the sand waves calculated from the crests and troughs. This information was then imported back into ArcMap™ (Fig. 5). In ArcMap™, the sand wave crests were delineated along those crests points imported from MatLab®. This methodology incorporates a level of automation to ensure sand waves were not overlooked due to subjective assessment on the part of the author. However, the final decision to classify a feature as a sand wave is still based on the judgment of the author, which allowed the flexibility to incorporate other information such as seafloor aspect or slope.

After each crest was delineated, the sand wave height and wavelength values of the crest-points along the sand wave crest were tabulated. Each sand wave was assigned an average, maximum, and minimum height and wavelength. The standard deviation of sand wave height and wavelength indicates variation along the sand wave. Sand wave orientation was determined by examining the slope on either side of the crest and the shape of the sand wave in cross section, and then classified as flood- or ebb-dominant.

3.2. Current

Two Sontek Argonaut SL current meters were deployed from 15 July to 26 August 2005 (Fig. 2). The readings were taken about 1 m above the seabed, and 2-min averages were recorded every 5 min. The data from these meters were downloaded weekly, and the meters were immediately redeployed. Some shift in position occurred during each redeployment, on the order of 50–75 m. One meter was deliberately moved twice to avoid areas of heavy boat traffic, and the other had to be moved three times. The current record is not continuous for either meter due to instrument disturbance.

3.3. Tide

A MacroTide tide gauge was deployed throughout the field campaign. The instrument was located east of the survey area in about 2 m of water (Fig. 2). The instrument was placed in shallow water so that data could be downloaded each week without disturbing the instrument. The observed spring tidal range is about 1 m and the neap range is about 60 cm. The record shows a diurnal inequality of about 20 cm.

3.4. Bedload transport

Movement of sand will occur if shear stress exceeds the critical shear stress. The critical shear stress depends on the grain size and water depth. Calculation of shear stress in the study was determined by first finding the shear velocity, and then using density of water to determine the shear stress. The potential bedload transport rate can be evaluated theoretically. First, van Rijn's (1984b) derivation of the critical velocity was applied to the study site (van Rijn, 1984b). This formula (Eq. (1)) uses the flow depth and grain size to estimate the velocity at which sediment transport begins:

$$\begin{aligned}\overline{U_{cr}} &= 0.19(d_{50})^{0.1}\log\left(\frac{4h}{d_{90}}\right) \text{for } 0.1 \text{ mm} \le d_{50} \le 0.5 \text{ mm}\\ \overline{U_{cr}} &= 8.5(d_{50})^{0.6}\log\left(\frac{4h}{d_{90}}\right) \text{for } 0.5 \text{ mm} \le d_{50} \le 2 \text{ mm}\end{aligned} \quad (1)$$

in which $\overline{U}_{cr}$ is the critical velocity of sediment movement in meters per second, d_{50} is the median grain size in meters, d_{90} is the grain size in meters for which 90% of the sample is finer than, and h is the water depth in meters.

The Meyer-Peter and Muller (MPM) (1948) and the van Rijn (1984a) formulas are two of the more well-known bedload transport equations (van den Berg, 1987; Madsen, 1993; Soulsby, 1997). MPM is one of the simplest bedload equations (Eq. (2)). It was empirically derived from flume experiments and is based on the concept of excess shear stress:

$$q_b = 8(\theta - \theta_{cr})^{3/2}\sqrt{g(s-1)d^3} \quad (2)$$

in which q_b is the volumetric bedload sediment transport rate, θ is the Shields parameter, θ_{cr} is the critical Shields parameter, g is acceleration due to gravity, s is the ratio of densities of sediment and water, and d is the grain diameter.

Conceptually, van Rijn begins his derivation with the idea that the bedload transport is equal to the product of the particle velocity, height of the saltation layer, and the concentration of the bedload particles. Eq. (3) is derived based on measured bedload transport rates and validated with field and flume data.

$$q_b = F_R\theta^{1/2}\left(\theta^{1/2} - \theta_{cr}^{1/2}\right)^{2.4}\sqrt{g(s-1)d^3} \quad (3)$$

Field measurements needed to apply these models included flow depth, grain size, and current speed. Representative values of grain size (0.4 mm) and depth (2.9 m) were chosen because these are the mean values of the sand wave field. The measured current velocities

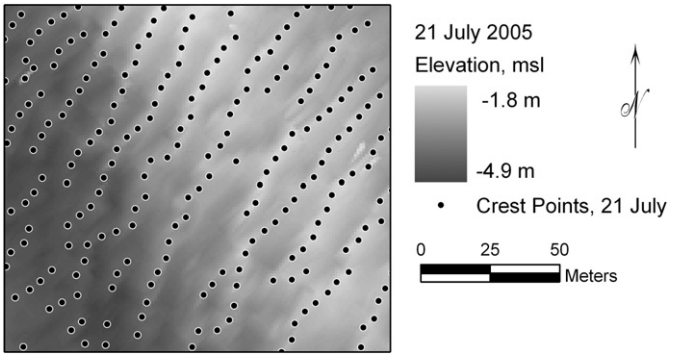

Fig. 5. Detailed bathymetric map with crests points (identified in MatLab®) superimposed. It is along these points that the crests (line features) are delineated.

were used to calculate the shear stress. The Shield Parameter was then calculated from the shear stress and applied in the models. Current velocities for the bedload calculation were those recorded by current meter EE85 (see Fig. 2). To develop a continuous record for the duration of the current meter deployment (14 July–14 August), the records from all the deployments were merged, and the gaps in the data were filled by modeling the tidal signal. A least-square cosine fit was used to model the missing data. The amplitudes and phase of eight cosines, representing eight tidal constituents (M2, S2, N2, K2, K1, O1, P1, MF) were calculated and applied to the velocity model (Fig. 6). The model was limited to eight constituents because this produced a good correlation between the observed and modeled velocities, with an *R*-squared value of 0.92. The time step for the bedload transport calculation was 15 min. Ebb velocity was negative and flood was positive so the net, as well as the gross, transport could be evaluated.

Bedload transport may be estimated from sand wave migration Soulsby (1997):

$$q_b = a_m \eta U_m \tag{4}$$

where η is the height of the sand wave, U_m migration speed of the sand wave, and the quantity a_m is a constant based on the porosity and the shape of the sand wave. Because the porosity was unknown, a default value of 0.32 was used (Jinichi, 1992). In this study, Eq. (4) was used to calculate migration velocity of the sand waves based on the calculated bedload transport rate:

$$U_m = \frac{q_b}{a_m \eta} \tag{5}$$

4. Results

4.1. Sediment

The sand wave field is covered with moderately well-sorted, medium- to coarse-grain sand. Twenty-two sediment samples were collected from the sand wave field and the surrounding areas (Fig. 2). The grain size within the sand wave field (0.36 mm) is slightly smaller than the grain size of the sediment outside the sand wave field (0.46 mm). The difference between the mean and median grain size for the five samples collected within the sand wave field was 0.01 mm. Therefore, either value may represent the sediment distribution equally well.

4.2. Tide

Mean sea level, as calculated from the tide data collected for this study, was −0.10 m NAVD88 (±0.07 m) (*N*orth *A*merican *V*ertical *D*atum). Tide harmonics were calculated with SimplyTides (Boon, 2004). Analysis of the data from Moriches Inlet shows the M_2 component to be 31 cm. Defant's form number is 0.28, falling just into the mixed, predominantly semidiurnal category. The M_4/M_2 phase shift, 2.1 rad, indicates an ebb-dominance, but the ratio of the M_4/M_2 amplitudes, 0.03, shows this dominance is slight. Velocity data collected in the field indicate this area is flood-dominant.

4.3. Currents

Tidal currents flow parallel to the channel and normal to the sand wave crests. Peak current velocity reached just over 50 cm/s, and the greatest velocity recorded was 60 cm/s. Over all, the study area is

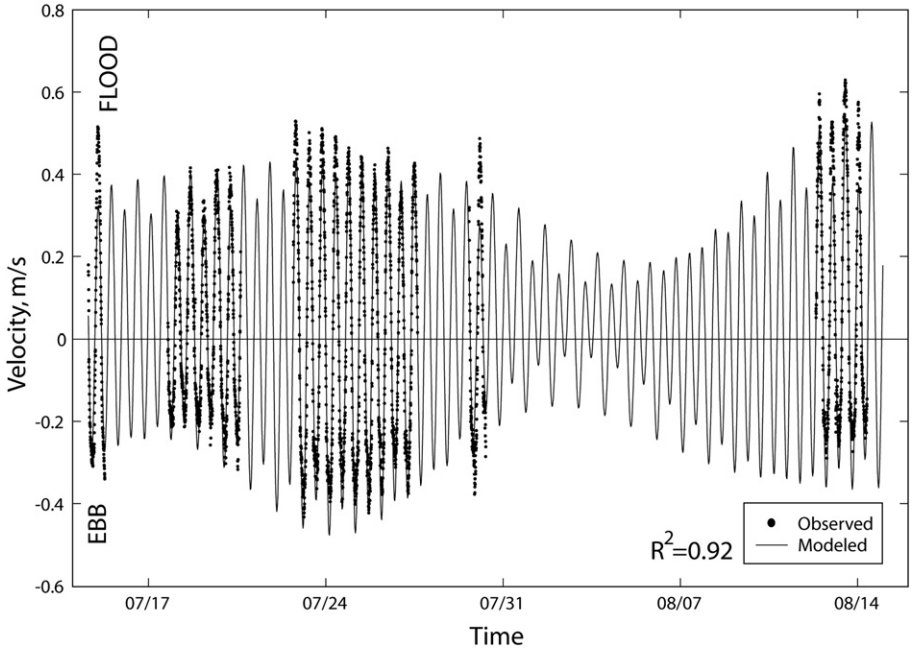

Fig. 6. Measured and modeled velocity data. The model data are the values used in the bedload transport calculation. Meter EE54 was used rather than EE85 because EE54 was generally located on the east side of the study area closer to the sand wave field. Neither meter was located directly within the sand wave field because it was shallow and inline with boat traffic.

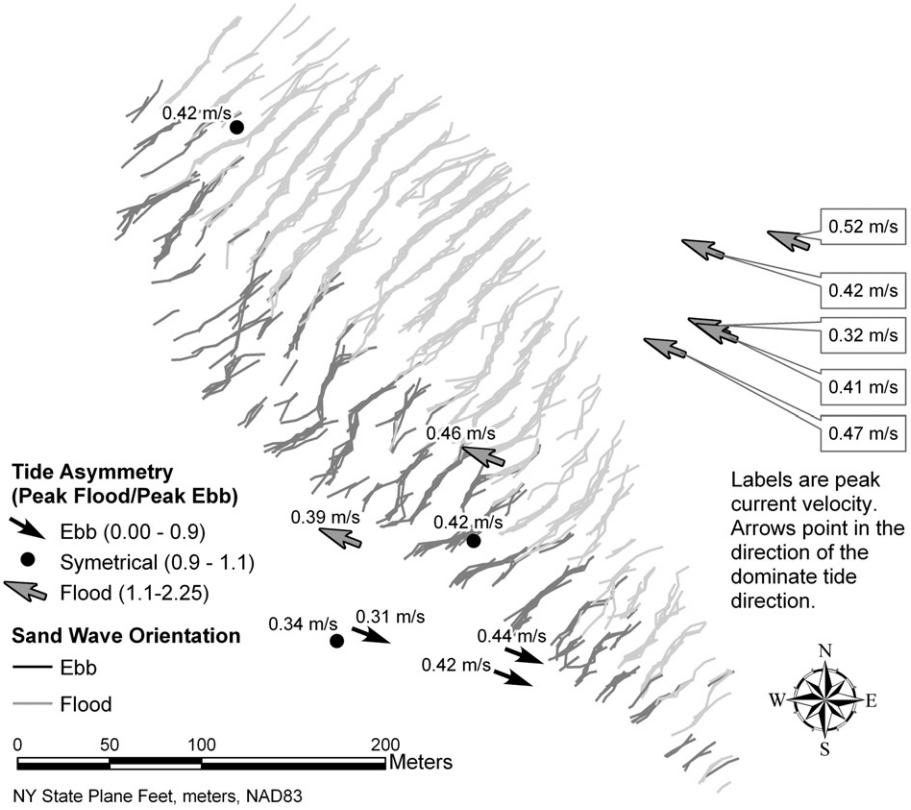

Fig. 7. Peak measured current velocity. Locations are labeled with the peak current speed. The arrows point in the direction of the dominant current. Tide asymmetry is defined as the ratio between the peak flood current and the peak ebb current. Ratios greater than 1 are flood-dominant and those less than 1 are ebb-dominant. There were only three ebb-dominant records, which were collected in the southwest corner. The sand wave orientation data presented here is discussed in the next section. It is shown here for reference.

flood-dominant with stronger flood current, 52 cm/s, and a shorter flood duration, 5.57 h, compared to the weaker ebb current of 44 cm/s and longer ebb duration of 6.40 h. However, the current velocity and tidal duration vary at each station; peak ebb current ranges from 20–44 cm/s, and the peak flood current ranges from 7–52 cm/s.

Flow in the study area is characterized by two mutually exclusive tidal channels. The current records from the east side of the study area are flood-dominant whereas the southern location is ebb-dominant (Fig. 7). The study area is mostly flood-dominant except for the southwestern portion.

4.4. Sand wave morphology

Bathymetric surveys within the 0.07 km^2 study area show two unique morphologies—the larger, better-defined, flood-dominant sand waves on the shallow bank, and smaller, ebb-dominant sand waves in the ebb channel. The mean height was 39 cm and the wave length was 15 m over the entire study area. The mean height for an individual survey ranged from 37 to 41 cm and the mean length ranged from 14.4 to 16.7 m over the study period. The sand waves did not to respond to changes in flow conditions between neap and spring fortnightly cycles. The average spacing of the ebb- and flood-orientated sand waves was the same, but their heights varied. The ebb-orientated sand wave height was 23 cm compared to the larger flood-orientated sand wave height that was 46 cm.

Asymmetrical sand waves have a slip face which faces the direction of migration. The orientation of the slip face is a morphological indicator of net sediment transport direction. The pattern of sand wave orientation supports the existence of two mutually exclusive tidal channels, similar to the channels identified in the current record. The eight weekly surveys were taken at various stages of ebb and flood tides. Regardless of the tide stage, the same sand wave orientation pattern emerged in every survey (Fig. 8). Sand waves on the shallower bank in the center of the study area are flood-orientated, and those in the western channel are ebb-orientated.

To determine the detailed characteristics of the sand waves, a more comprehensive analysis was preformed on five flood-orientated sand waves from the bank region. These sand waves were chosen for this analysis because they were larger than average, uniformly spaced, and had well-defined slip faces. The wavelength, height, slope, and location of the sand waves were analyzed. The height of these sand waves ranged between 34 and 43 cm. The variability (standard deviation) of the height along the sand wave is on the same order of magnitude as the change in height over time. The wavelength ranged from 11 m to 13 m. Again, the standard deviation of the wavelength along the crest is similar to the variation over time.

The slip face slope of the sand waves was measured as the average angle between the crest and trough. The slopes are shallow, varying from 3.6° to 4.4°, when measured from crest to trough (Fig. 9). There are localized sections of the slip face that may approach 10°. The northwest slope was steeper, indicating flood-dominance, in all cases except for two-sand waves on 19 August 2005. However, on the two occasions when the sand wave asymmetry reversed, the difference between the northwest and the southeast slope was only 0.1°, which is within the error of this analysis so the change in orientation is not conclusive.

4.5. Sand wave size predictions

Laboratory studies (Southard, 1971; Southard and Boguchwal, 1990a) and field investigations (Yalin, 1964; McCave, 1971; Boothroyd and Hubbard, 1975; Dalrymple et al., 1978; Zarillo, 1982; van Rijn, 1984b; Aliotta and Perillo, 1987; Gabel, 1993; Dalrymple and Rhodes, 1995; Mazumder, 2003) have demonstrated that bedform

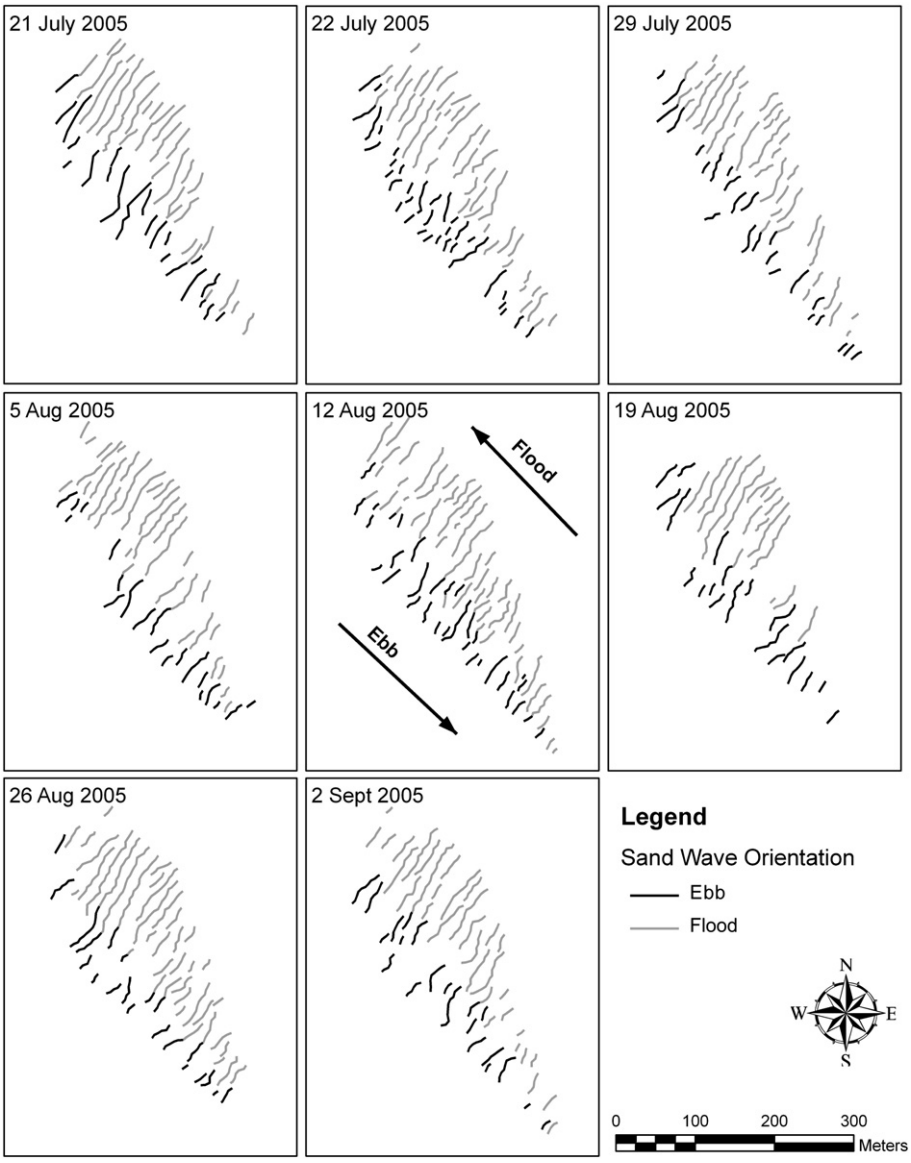

Fig. 8. Sand wave orientation for the eight surveys. Lines indicate the location of sand wave crests; grey are flood-orientated, and black are ebb-orientated. Flood-dominant sand waves occupy the shallow portion of the bank, while the sand waves in the western channel are ebb-dominant, in line with the tidal asymmetry in each region.

morphology is a function of flow depth, grain size, and flow velocity or shear stress. van Rijn (1984b) has modeled sand wave height based on the shear stress, grain size, whereas wavelength is based only on water depth. van Rijn's relationships are:

$$\eta = 0.11h\left(\frac{d_{50}}{h}\right)^{0.3}\left(1-e^{-0.5T_s}\right)(25-T_s) \quad \tau_{cr}<\tau<26\tau_{cr} \tag{6}$$

where

$$T_s = \frac{\tau-\tau_{cr}}{\tau_{cr}} \tag{7}$$

$$\lambda = 7.3h \tag{8}$$

τ is the shear stress, τ_{cr} is the critical shear stress, and λ is the sand wave spacing. The model predicts that no sand waves would develop if the shear stress is less than the critical value ($\tau<\tau_{cr}$) because there would be no sediment transport under these conditions. van Rijn (1984b) also acknowledges a maximum shear stress beyond which bedforms are 'washed out.' Using values representative of the Moriches Inlet field site (d_{50}=0.48 mm and h=3 m), the height and length of the sand waves can be estimated. The shear stress was evaluated for a current velocity of 0.4 m/s, 0.5 m/s, and 0.6 m/s (Table 2). The wavelength predictions are larger than observations, 22 m compared to an observed average wavelength of 15 m. The standard deviation of the observed wave lengths is 4 m, so the wavelength is over predicted. Sand wave height is consistently under-predicted (2–29 cm) compared to observations of 39 cm. The standard deviation of the sand wave heights measured at the study area is 13 cm. Again, the predicted and observed values agree, albeit just barely.

Published studies indicate that the height and wavelength of sand waves are directly related. Dalrymple et al. (1978) and Flemming (1988) both proposed relationships between these dimensions based on measurements from the Bay of Fundy, and flume and river data, respectively. Flemming's equation:

$$\eta_{min} = 0.0677\lambda^{0.8098} \tag{9}$$

$$\eta_{max} = 0.16\lambda^{0.84} \tag{10}$$

Dalrymple's equation:

$$\eta = 0.0635\lambda^{0.733} \tag{11}$$

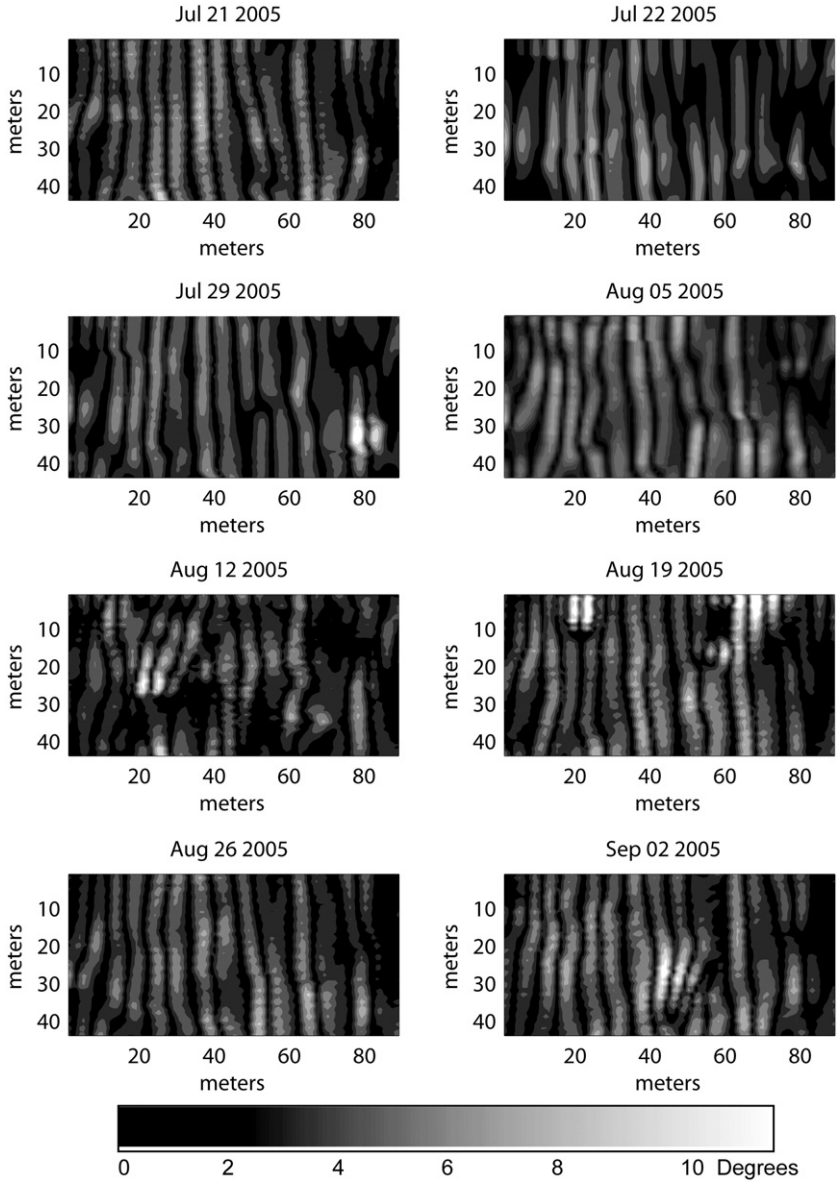

Fig. 9. Slope of the normalized bathymetry in the detailed study area.

Both relationships over estimate the sand wave height (Fig. 10). Based on the average sand wave length observed at Moriches Inlet (15 m), Dalrymple's equation predicts a sand wave height of 46 cm, and Flemming's relation predicts heights between 60 cm and 1.5 m. The scatter in the data seems random, and there appears to be no correlation between sand wave height and wavelength.

4.6. Sand wave movement

The location of the sand wave crests was tracked over the eight-week study (Fig. 11). Considering the horizontal uncertainty of the depth soundings (±1 m), these data indicate a lack of systematic migration of the sand waves over the study period. Realignment, flexing, and some bifurcation of the crests occurred. However, bifurcating crests usually returned to their previous continuous configuration and therefore, may be the result of variations in interpolation due to differences in the location of the soundings between surveys rather than changes in the morphology. This analysis clearly illustrates that the sand waves are immobile under the conditions that were monitored during this study.

4.7. Bedload transport

MPM and van Rijn's bedload transport equations were applied to Moriches Inlet (Eqs. (2) and (3)). The resulting gross bedload transport is 0.06 m^3/m for MPM and 0.02 m^3/m for van Rijn for the duration of the measurement period (15 July–14 August). The net transport in the flood direction is 0.03 m^3/m for MPM and 0.01 m^3/m for van Rijn. Critical velocity for the initiation of sediment movement was 37 cm/s, which was exceeded only 7% of the time (Fig. 12).

Table 2
Predicted sand wave heights and wavelength

	$\overline{U}$=0.4 m/s	$\overline{U}$=0.5 m/s	$\overline{U}$=0.6 m/s
Shear stress [N/m^2]	0.28	0.43	0.62
van Rijn height [m]	0.02	0.17	0.29
van Rijn wavelength [m]	22		

$\overline{U}$ is the depth-averaged velocity.

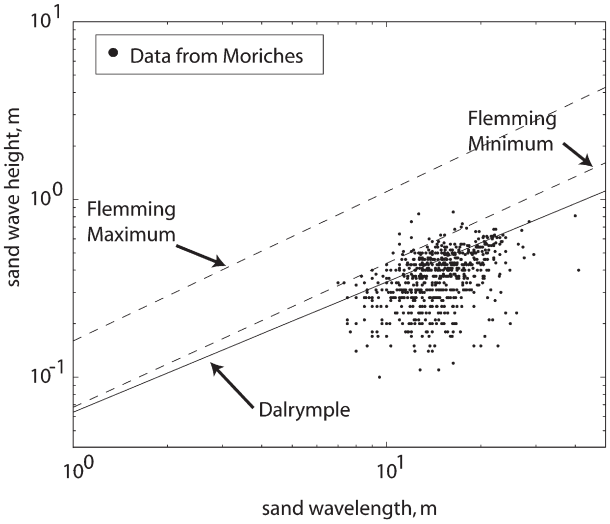

Fig. 10. Plot of sand wave height versus sand wave length. Data from Moriches Inlet are plotted as points. Superimposed on the data from Moriches Inlet are the length/height relationships proposed by Flemming (1988) and Dalrymple et al. (1978). Most of the data for Moriches Inlet plot below the proposed relationships. Dalrymple, who used field data in his derivation, fits the Moriches Inlet data better.

Based on the theoretical bedload transport rates, the potential sand wave migration was estimated. The net sand wave migration distance, based on the calculated bedload transport rate, should have been 0.19 m for MPM and 0.09 m for van Rijn (Eq. (5)). The gross migration distances were 0.40 m (MPM) and 0.15 m (van Rijn). Both estimates are less than the uncertainty of the bathymetric surveys and therefore should not have resulted in migration which could be tracked on our surveys.

5. Discussion

5.1. Morphology

Sand wave field in the eastern flood channel of Moriches Inlet is morphologically different from many other published observations in that they have gently sloping slip faces and are relatively flat. Many tidal sand waves have slip faces of ~15° (Harvey, 1966; Ludwick, 1970; Bokuniewicz et al., 1977; Langhorne, 1982; Dalrymple, 1984; Dalrymple and Rhodes, 1995; Fenster et al., 2006), whereas, the slip faces measured in this study were only 3.6°–4.4°. Actively migrating sand waves tend to have a steeper slip face because sand is deposited on the upper portion of the lee slope as it is eroded from the stoss side transported over the crest, thus increasing the slope until it becomes unstable and avalanching begins. Therefore, it can be reasoned that sand waves with shallow slip faces, such as those at Moriches Inlet, are either not migrating, migrate very slowly, or migrating sporadically.

Low-angle sand waves are not unique to Moriches Inlet. They have been reported in other areas such as the River Rhine (Carling et al., 2000), the North Sea (van Dijk and Kleinhans, 2005), and the Fraser River (Kostaschuk and Villard, 1996). Because their morphology is unexpected, researchers have proposed various explanations for their occurrence:

1. *Shallow Water Depths*: When depths are shallow relative to the height of the sand wave ($\eta/h > 0.167$) (Yalin, 1964, 1977), the height of the sand wave may be limited by the water depth. Depth-limited sand waves have small heights compared to their wavelengths and, therefore, do not reach maximum steepness (Carling et al., 2000).
2. *Suspended Sediment*: High concentrations of suspended transport may deposit sand on the lower slip face or trough and decrease the slip face angle (Julien and Klaassen, 1995; Kostaschuk and Villard, 1996).
3. *Symmetrical Flow*: Sand waves under symmetrical flow conditions may have a centrally located crest and, therefore, more equal angles on both sides, thus causing the slip face to be less steep (Allen, 1980).
4. *Waves*: Waves may erode the sand wave crests, making the sand waves flatter (Dalrymple and Rhodes, 1995).
5. *Supercritical Flow*: When flow conditions approach supercritical (Froude number >0.8) the height of sand waves will decrease as the sand waves become unstable and are replaced by an upper plane bed (Julien and Klaassen, 1995).

High concentrations of suspended sediment, waves, and supercritical flow are unlikely to cause the shallow slip face angles at Moriches Inlet because wave energy and sediment transport is minimal. However, the gentle slopes may be a factor of symmetrical flow or shallow water depths.

There are three important inferences that can be made based on the shallow slope of the sand waves. First, it is probable that sand may be transported in both directions, because the slip face does not act as a barrier for transport during the subordinate tide. Second, it is unlikely any migration occurs, because the slip face would be steeper if there were active migration. Finally, the sand waves at Moriches Inlet may be in a diminishing phase rather than a developing phase. Decay of sand waves in the River Rhine was described by Ten Brinke et al., (1999) and Wilbers and Ten Brinke (2003) occurring after passage of the peak discharge. This process generally involves a reduction in sand wave height, while the wavelength remains constant (Ten Brinke et al., 1999) or increases (Wilbers and Ten Brinke, 2003). This process results in an unusually low amplitude sand wave and, therefore, a gently sloped slip face.

The life-cycle of a sand wave under unsteady flow conditions can be divided into two phases—a developing phase and a diminishing phase. During the developing phase, the current velocity is increasing, and sand wave height and length are increasing as the system works toward equilibrium with the current. After the peak current velocity subsides, the sand waves enter the diminishing phase. During this phase the sand wave height decreases as the morphology seeks new equilibrium with the weaker current. This phase is usually associated with a change in height rather than length because less sediment transport is required to alter the height than the length. The sand waves at Moriches Inlet may be in a diminishing phase, similar to the sand waves in rivers after a period of high discharge. In this analogy, the high flow event may have occurred when the meteorological conditions increased the tidal range. During that time, the sand waves developed and were actively migrating. Subsequent to this event, the hydrodynamic conditions returned to the typical, less energetic conditions, and the sand waves entered the diminishing phase.

5.2. Dynamics

Observations of sand wave migration have been reported from many areas. Migration rates vary from 100 m/yr (Stewart and Jordan, 1964) to less than 5 m/yr (Salsman et al., 1966; Fenster et al., 2006), and still other studies have found no migration (Anthony and Leth, 2002). There was no net migration documented at Moriches Inlet during this study.

Sand wave migration is a function of the net sediment transport and sand wave size. Sand waves migrate faster as the net sediment transport increases and size decreases. In turn, net sediment transport and sand wave size are a function of water depth, current speed, and grain size. The *measured* migration rate also depends on the duration of the study and the accuracy of the equipment. If the duration of the study is too short or the resolution of the data is too large, migration may not be noticed. Observations from Moriches Inlet may be limited by the accuracy of the bathymetric surveys and the duration of the study. It is possible that longer monitoring of the sand wave field may

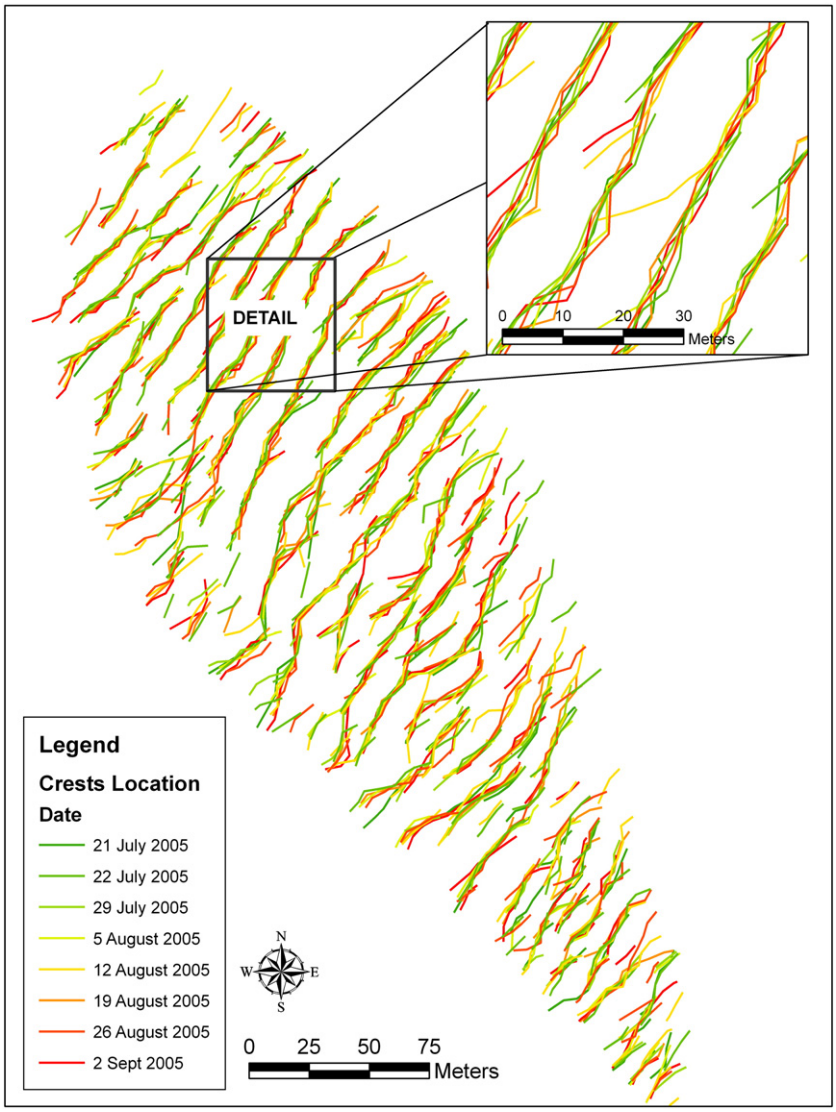

Fig. 11. Lines show location of sand wave crests from 21 July to 2 September 2005. There is some movement due to reworking of the sand waves and uncertainty in the surveys but there is no systematic movement of the sand waves indicating migration.

have recorded migration, more accurate surveys may have recorded finer scale movement, or data collected over the same time span but during more energetic conditions may have documented sand wave migration. Regardless, there was no migration greater than 2 m, the accuracy of the survey, during the two-month study period.

Intertidal sand waves on the flood deltas at the Essex and Parker Estuaries (70.77°W, 42.98°N) are 8–20 m long and 15–40 cm high (Boothroyd and Hubbard, 1974; Boothroyd and Hubbard, 1975), similar to those at Moriches Inlet. The grain sizes of the sediment (0.31–0.38 mm) comprising the sand waves were also comparable to those at Moriches Inlet. However, these features migrated 16–18 m over just three months. This may be attributed to the difference in current flow between the inlets. At the Essex and Parker Estuaries, the current speed reached 80 cm/s in areas with sand waves and the current was strongly flood-dominant, the ebb current only reached 40 cm/s. Divers observed that sand wave migration was initiated when the current speed exceeded 60 cm/s. The current velocity at Moriches Inlet study site rarely exceeds 60 cm/s. Faster current speeds and a larger difference between the peak ebb and flood current velocity result in faster migration rates at the Parker and Essex Estuaries than observed at Moriches Inlet.

Sand wave asymmetry may not be an accurate predictor of short-term migration rates at Moriches Inlet, but it may still be an accurate indicator of slow, long-term migration or episodic migration. Fenster et al. (1990) conducted two field studies in Long Island Sound. Their first study, which tracked the sand waves over seven months, documented no net migration, but did identify asymmetrical sand waves. However, 16 yr later they resurveyed the same area, and the sand waves had migrated an average of 35 m. It is unclear whether this migration was the result of persistent, slow migration or if migration occurred during episodic storm events because there were no intermediate surveys to document the rate of migration. At Moriches Inlet, the asymmetry in the sand wave morphology is likely a result of migration even though migration was not observed during this study.

Some insight to the migration patterns of the sand wave at Moriches Inlet may be gained through and investigation of the theoretical bedload transport rates. Given the typical grain size and depth at Moriches Inlet sediment transport is expected to occur when the current exceeds 37 cm/s (Eq. (1)). The current velocity exceeded this threshold only 7% of the time. The bedload transport in Moriches Inlet was calculated using MPM's and van Rijn's equations (Eqs. (2) and (3)). Both results indicate a low transport rate (0.02–0.03 m^3/m), which corresponds to a theoretical net migration of 9 to 19 cm (Eq. (5)) from 14 July to 14 August, for van Rijn and MPM respectively. This calculation is consistent with the field observations.

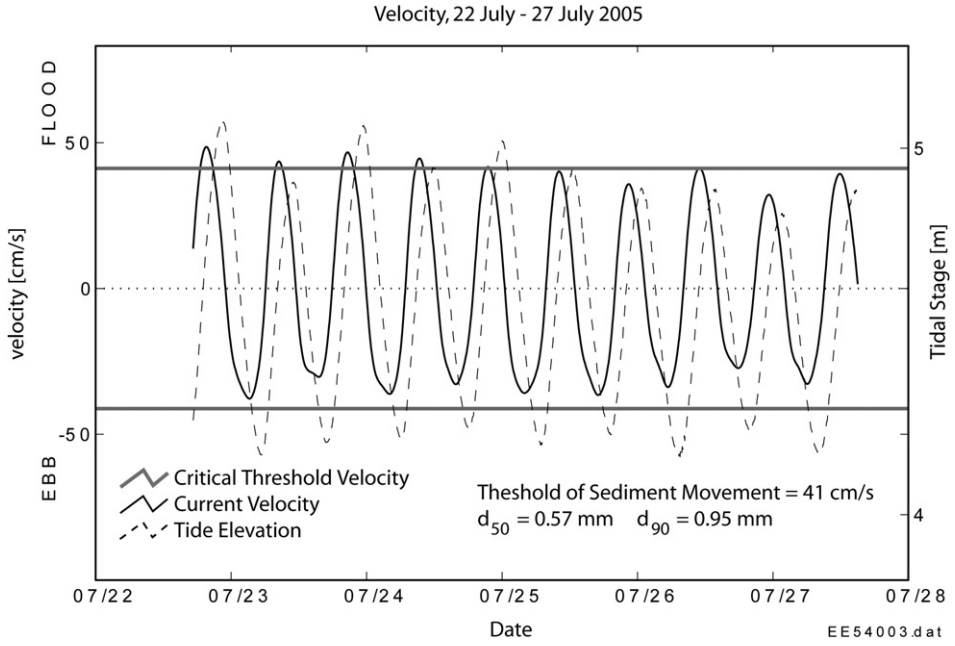

Fig. 12. This plot is an example current meter record. The bold grey line shows the critical velocity which must be exceeded to initiate sediment transport. As shown in this example the critical threshold is not often exceeded.

5.3. Sand wave development

5.3.1. Relic sand waves

The sand wave field at Moriches Inlet has been identified on aerial photographs from 2001 and 2004, and bathymetric surveys from 2004 and 2005. Sand wave spacing has been consistent since 2001. The height of the sand waves could not be measured from the aerial photographs.

The development of sand waves is a function of water depth, flow velocity, and sediment characteristics, as well as the availability of

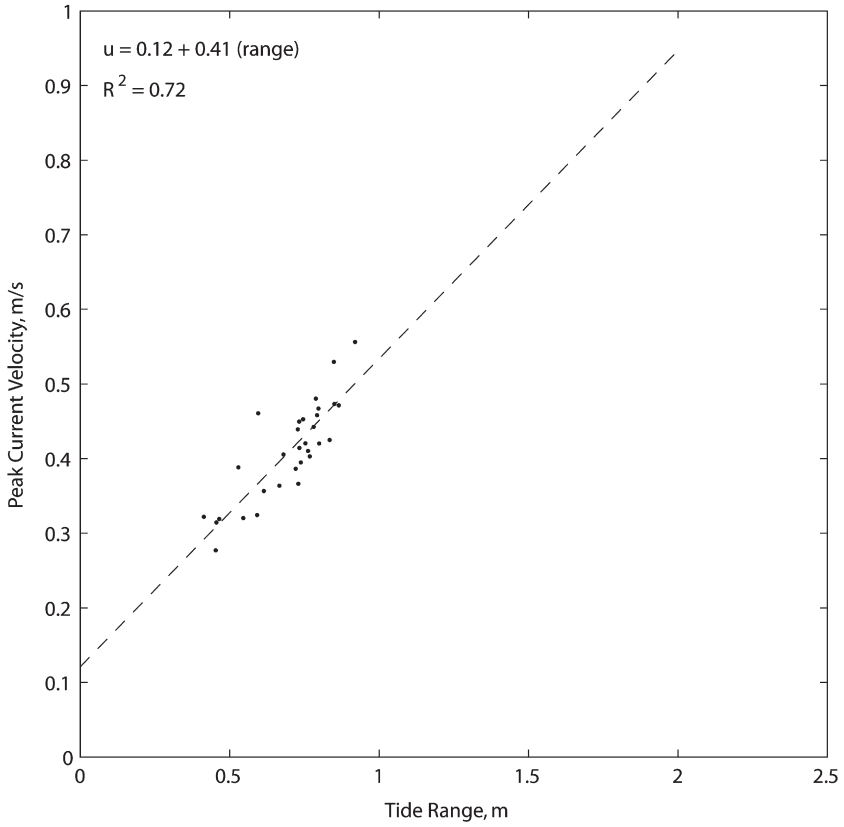

Fig. 13. Generalized regression analysis for Moriches Inlet.

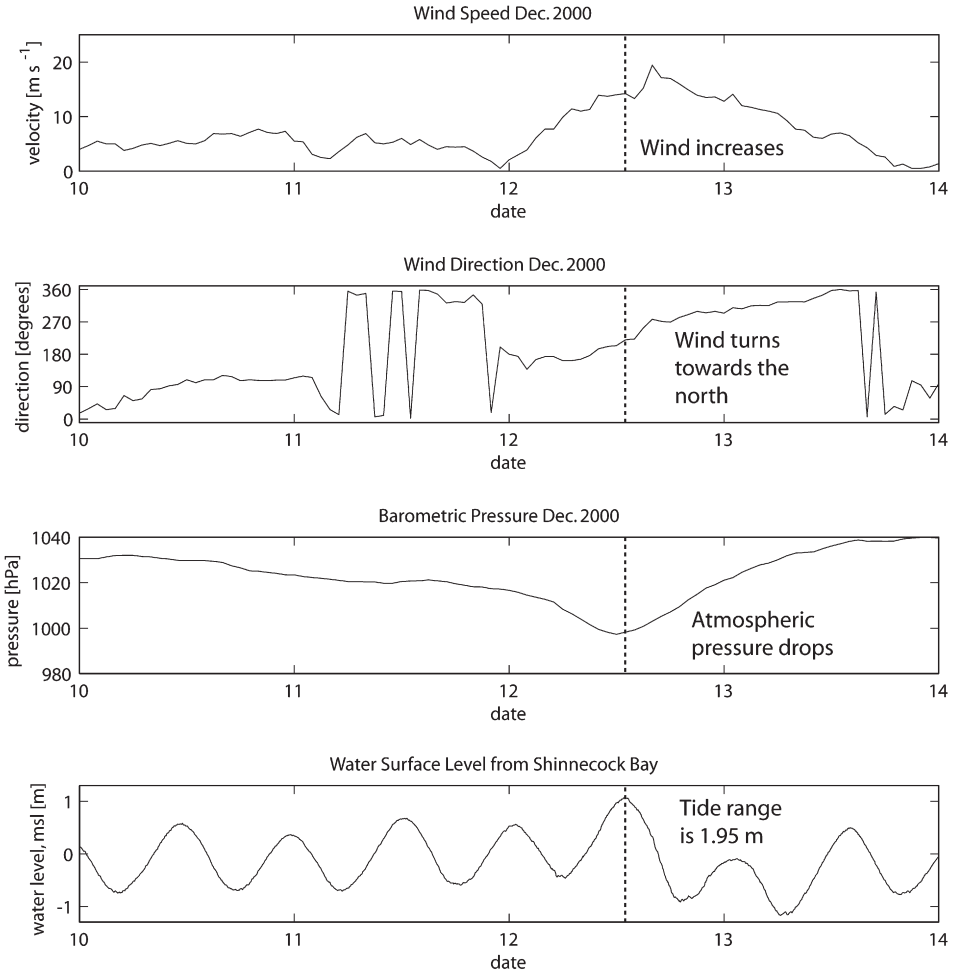

Fig. 14. Wind speed and direction, barometric pressure, and water level at Shinnecock Inlet 10 December–14 December 2000. Wind data are from the National Data Buoy Center (Station 44025) and the water level data are from the LIShore Shinnecock Bay tide gauge.

sand, dredging, and wave action. Predictions of sand wave height based on flow velocity measured at Moriches Inlet (van Rijn Eq. (6)) under predict the height of the sand waves, suggesting that a stronger current velocity was responsible for building these features. Assuming these predictions are accurate, the flow conditions responsible for creating these features were likely not observed during this study.

Evidence for sand wave development under conditions different than those seen during this study is also evident in the slope of the slip face. The sand waves display an asymmetrical profile, but the slip face is gently sloped and does not approach the angle of repose. Likely, sand waves were actively migrating during their developing phase, but are now stationary because the net sediment transport is not sufficient to cause migration. The weak current and minor sediment transport have modified the slope of the sand waves, but is not sufficient to erode them.

The sand waves at Moriches Inlet are less steep than observations made by Flemming (1988) and Dalrymple et al. (1978). Predictions of sand wave height based on wavelength (Fig. 10) over predict the height. During the diminishing phase sand wave height will decrease faster than the wavelength because less sediment transport is needed to alter the height. Therefore, the steepness of the sand wave decreases. The elongate wavelength relative to the height indicated that these sand waves are in a diminishing phase.

5.3.2. Estimation of current velocity during development

Given the reasons described above, it is concluded that the sand wave field at Moriches Inlet developed when flow conditions where stronger than those observed during this study, possibly during a storm surge or other meteorological event that increased the tidal current velocity. Since then, the typical flow conditions have gently reworked the sand waves, relocating the crests to a more central location, and flattening the slip face while the sand waves remain stationary.

The theoretical event creating the sand waves can be reconstructed using the empirical equations for sand wave height published by van Rijn (1984b) and the physical relationship between tidal range and current speed. The observed sand wave height is 39 cm. To achieve this height, according to the relationship published by van Rijn (1984b), the current speed should be at least 80 cm/s. Therefore, it can be assumed that the event creating these sand waves caused the current velocity in the study area to increase to 80 cm/s.

The velocity of the tidal current is a function of the tidal prism and period. Because the tidal period remains constant, as the tidal prism increases, the water must flow faster in order to accommodate the larger flux. As long as the area of the bay remains constant as the water level rises, tidal range is a valid proxy for tidal prism. In a bay with steep sides and few tidal flats, such as Moriches Bay, the area of the bay remains fairly constant throughout the tidal cycle and, therefore, the relation between tidal prism and current speed can be extrapolated to tidal range and current speed. The velocity data collected during this study indicates that the bay area remains constant as the water elevation nears high tide. The velocity gradually decreases near high tide; if there were large increases in the bay area as the water level rose and flooded the tidal flats the velocity record would show an in acceleration near high tide but it does not.

Variations in tidal range, which may be caused by changes in meteorological conditions, can enhance or retard the tidal signature.

For example, during a storm, low barometric pressure, wave setup, and wind forcing may increase or decrease the elevation of the water's surface. This change may increase the tidal range and, therefore, the current velocity.

The water level and current data collected at Moriches Inlet were used to calculate the tidal range and the associated peak current speed so that a relationship between these two parameters could be defined. The linear regression between peak current speed and tidal range was calculated for three records. Other current records were discarded because of the poor data quality (high signal-to-noise ratio or invalid velocities because the meter tipped over) or the length of the record (at least four days of measurements were needed). The flood velocities were stronger and showed a better correlation to tidal range than did the ebb velocities so the flood data were used. A generalized relation between tide range and peak current velocity for the study area was obtained from these three stations (Fig. 13):

$$U_{\text{peak}} = 0.12 + 0.41\ (\text{Tidal Range}) \tag{12}$$

where U_{peak} is the peak tidal current in m/s. The R-squared value ranged from 0.73 to 0.94 for the individual stations, and was 0.72 for the generalized relationship. The generalized relationship was used to predict the tidal range. Based on the regression, the peak current velocity will be 80 cm/s when the tidal range reaches 1.66 m.

5.3.3. Hypothetical event creating sand waves

Water level data from Sandy Hook, NJ[2] and Shinnecock Bay, NY[3] were analyzed to evaluate the frequency of events with a tidal range exceeding 1.66 m. Shinnecock Inlet is 30 km east of Moriches Inlet, and the tide gauge was just inside the inlet. Sandy Hook is the NOAA reference station for Moriches Inlet. The correction for low water is 0.60, and the correction for high water is 0.62. These corrections were applied to the observed water levels measured at Sandy Hook to approximate the tidal range at Moriches Inlet. Between May 1998 and December 2005, the tidal range exceeded 1.66 m only once, on 12 December 2000. This tidal range could have increased the tidal velocity and created the sand wave field at Moriches Inlet. During that day, the wind velocity increased from 2 m/s to 19 m/s, and the wind changed from the southwest to the north (Fig. 14). In addition, the barometric pressure dropped below 1000 pHa. The drop in atmospheric pressure raised the elevation of the high tide and the wind enhanced the ebb flow out of the bay creating an extra low low-tide. The result was an extremely large tidal range of 1.95 m (spring range is 1 m), which corresponds to a predicted current velocity of 0.92 m/s.

A historical analysis of the Sandy Hook tide gauge from 1990 through 2005 shows that events like this one, exceeding 1.66 m, are expected only once every 8 yr. Perhaps not often enough to maintain the sand wave field, but it may be enough to create the sand waves which may be maintained by weaker flow. Smaller increases in tidal range are more common and may be critical in maintaining the sand waves. Boothroyd and Hubbard (1974) recorded sand wave migration when current velocity exceeded 60 cm/s. At Moriches Inlet, this flow velocity is predicted to occur when the tidal range reaches 1.17 m. Analysis of the Sandy Hook tide gauge data show that this may occur as often as every three days, generally during the spring tide. The moderate energy events may be critical in maintaining this sand wave field.

6. Conclusions

Our understanding of the factors controlling the morphology and dynamics of sand waves has been expanded through a case study at Moriches Inlet. The collection of a detailed in situ data set allowed for the comparison of field data to previously published observations and morphologic models. Exploring the differences between the observations and predictions forced us to examine why these deviations occur.

The stability and morphology of sand waves monitored during a period of eight weeks at Moriches Inlet indicate that this is a relic sand wave field, created and maintained by episodic, high-energy events. Evidence for a relic sand wave field includes no migration, gentle slip face slopes, and uncommonly short sand waves. It is hypothesized that the sand wave field remains inactive until it is mobilized by an extreme flow event. Subsequent low-energy flow conditions help maintain or modify the sand waves but are insufficient to eliminate them. Under normal flow conditions, it is believed that low rates of bidirectional sediment transport reshape the sand waves, shifting the crest to a central location between the adjacent troughs and decreasing the lee slope. Flow separation over the sand wave crests likely does not occur due to their gentle slopes and low current velocities.

This conclusion is similar to the findings of Diesing et al. (2006) who were studying a sand wave field in the German Bight. Here they found that "extreme storm events may play a major role in the generation of sorted bedforms, whereas the quasi-continuous tidal currents form and maintain their final shape." Peak storm-driven currents are also responsible for the sand wave asymmetry on Sable Island Bank, Scotain Shelf (Li and King, 2007). Our major conclusion from this study is that sand waves in regions of low energy may be representative of infrequent high-energy events.

Acknowledgments

The authors would like to thank Drs. Kraus and Zarillo for their collaboration on this research. Their comments have greatly helped to elucidate the significance of this research. Shelley Whitmeyer would also like to acknowledge the Office of Naval Research for their support through the National Defense Sciences and Engineering Fellowship. Support provided by the Coastal Inlets Research Program, U.S. Army Corps of Engineers, in the form of technical advice, field equipment, and financial support for data collection has been critical to the completion of this research. In addition, the Geological Society of America has also provided financial support for data collection through their Graduate Student Research Grant.

References

Aliotta, S., Perillo, G.M.E., 1987. A sand wave field in the entrance to Bahia Blanca estuary, Argentina. Mar. Geol. 76, 1–14.
Allen, J.R.L., 1980. Sand waves: a model of origin and internal structure. Sediment. Geol. 26, 281–328.
Anthony, D., Leth, J.O., 2002. Large-scale bedforms, sediment distribution and sand mobility in the eastern North Sea off of the Danish west coast. Mar. Geol. 182 (3/4), 247–263.
Ashley, G.M., 1990. Classification of large-scale subaqueous bedforms: a new look at an old problem. J. Sediment. Petrol. 60 (1), 160–172.
Bartholdy, J., Bartholomae, A., Flemming, B.W., 2002. Grain-size control of large compound flow-transverse bedforms in a tidal inlet of the Danish Wadden Sea. Mar. Geol. 188, 391–413.
Bokuniewicz, H.J., Gordon, R.B., Kastens, K.A., 1977. Form and migration of sand waves in a large estuary, Long Island Sound. Mar. Geol. 24, 185–199.
Boon, J.D., 2004. Secrets of the Tide: Tide & Tidal Current Analysis and Predictions, Storm Surges, and Sea Level Trends. Horwood Publishing Limited. 300 pp.
Boothroyd, J.C., Hubbard, D.K., 1974. Bed form development and distribution pattern, Parker and Essex Estuaries, Massachusetts. Miscellaneous Paper 1-74. U.S. Army Corps of Engineers, Coastal Engineering Research Center, Fort Belvoir, VA.
Boothroyd, J.C., Hubbard, D.K., 1975. Genesis of bedforms in mesotidal estuaries. In: Cronin, L.E. (Ed.), Estuarine Research. Academic Press, Inc., New York, New York, pp. 217–234.
Carling, P.A., Golz, E., Orr, H.G., Radecki-Pawlik, A., 2000. The morphodynamics of fluvial sand dunes in the River Rhine, near Mainz, Germany. I. Sedimentology and morphology. Sedimentology 47, 227–252.
Dalrymple, R.W., 1984. Morphology and internal structure of sandwaves in the Bay of Fundy. Sedimentology 31, 365–382.

[2] NOAA Tide Station 8531680 (40° 28.0′ N, 74° 0.6′ W).
[3] The Shinnecock Bay tide gauge was maintained by the LIShore program under the direction of the USACE, Coastal Inlets Research Program.

Dalrymple, R.W., Rhodes, R.N., 1995. Estuarine dunes and bedforms. In: Perillo, G.M.E. (Ed.), Geomorphology and Sedimentology of Estuaries. Elsevier Science, pp. 359–422.
Dalrymple, R.W., Knight, J.R., Lambiase, J.J., 1978. Bedforms and their hydraulic stability relationships in a tidal environment, Bay of Fundy, Canada. Nature 275, 100–104.
Diesing, M., Kubicki, A., Winter, C., Schwarzer, K., 2006. Decadal scale stability of sorted bedforms, German Bight, southeastern North Sea. Cont. Shelf Res. 26 (8), 902–916.
Engelund, F., Fredsoe, J., 1982. Sediment ripples and dunes. Annu. Rev. Fluid Mech. 14, 13–37.
Ernstsen, V.B., Noormets, R., Winter, C., Hebbeln, D., 2005. Development of subaqueous barchanoid-shaped dunes due to lateral grain-size variability in a tidal inlet channel of the Danish Wadden Sea. J. Geophys. Res. 110.
Fenster, M.S., FitzGerald, D.M., Bohlen, W.F., Lewis, R.S., Baldwin, C.T., 1990. Stability of giant sand waves in Eastern Long Island Sound, U.S.A. Mar. Geol. 91, 207–225.
Fenster, M.S., FitzGerald, D.M., Moore, M.S., 2006. Assessing decadal-scale changes to a giant sand wave field in eastern Long Island Sound. Geology 34 (2), 89–92.
Flemming, B.W., 1988. Zur Klassifikation subaquatischer stromungstransversaler Transportkorper. Boch. Geol. Geotech. Arb. 29 (93–97).
Gabel, S.L., 1993. Geometry and kinematics of dunes during steady and unsteady flows in the Calamus River, Nebraska, U.S.A. Sedimentology 40, 237–269.
Granat, M.A., Alexander, M.P., 1991. Evaluation of an experimental jet fluidizer for removal of sand waves in the Columbia River. Report 2 1988 Exercise. U.S. Army Engineer Waterways Experiment Station, Vicksburg, MS.
Harvey, J.G., 1966. Large sand waves in the Irish Sea. Mar. Geol. 4 (1), 49–55.
Hoekstra, P., et al., 2004. Bedform migration and bedload transport on an intertidal shoal. Cont. Shelf Res. 24 (11), 1249–1269.
Hulscher, S., Dohmen-Janssen, C.M., 2005. Introduction to special section on marine sand wave and river dune dynamics. J. Geophys. Res.-Earth Surf. 110 (F4).
Jinichi, H., 1992. Application of sandwave measurements in calculating bed load discharge. Symposium on Erosion and Sediment Transport Monitoring Programmes in River Basins. International Association of Hydrological Sciences, Oslo, Wallingford, U.K., pp. 63–70.
Johnston, S., Kraus, N.C., Brown, M.E., Grosskopf, W.G., 2002. DMS: Diagnostic Modeling System, Report 4, Shoaling Analysis of St. Marys Entrance, Florida. U.S. Army Corps of Engineers, Engineer Research Development Center, Vicksburg, MS.
Julien, P.Y., Klaassen, G.J., 1995. Sand-dune geometry of large rivers during floods. J. Hydraul. Eng. 121 (9), 657–663.
Katoh, K., Kume, H., Kuroki, K., Hasegawa, J., 1998. The development of sand waves and the maintenance of navigation channels in the Bisanseto Sea. In: Edge, B.L. (Ed.), Coastal Engineering 1998. American Society of Civil Engineers, Copenhagen, Denmark, pp. 3490–3502.
Knaapen, M.A.F., Hulscher, S.J.M.H., 2002. Regeneration of sand waves after dredging. Coast. Eng. 46 (4), 277–289.
Kostaschuk, R., Villard, P., 1996. Flow and sediment transport over large subaqueous dunes: Fraser River, Canada. Sedimentology 43, 849–863.
Langhorne, D.N., 1982. A study of the dynamics of a marine sandwave. Sedimentology 29 (4), 571–594.
Levin, D.R., Lillycrop, W.J., Alexander, M.P., 1992. Sand Waves, Report 1, Sand Wave Shoaling in Navigation Channels. U.S. Army Engineer Waterways Experiment Station, Vicksburg, MS, p. 53.
Li, M.Z., King, E.L., 2007. Multibeam bathymetric investigations of the morphology of sand ridges and associated bedforms and their relation to storm processes, Sable Island Bank, Scotian Shelf. Mar. Geol. 243 (1–4), 200–228.
Lillycrop, W.J., Rosati, J.D., McGehee, D.D., 1989. A Study of Sand Waves in the Panama City, Florida, Entrance Channel. Coastal Engineering Research Center, Vicksburg, MS, p. 48.
Ludwick, J.C., 1970. Sand waves and tidal channel in the entrance to Chesapeake Bay. The Va. J. Sci. 21, 178–184.
Madsen, O.S., 1993. Sediment Transport on the Shelf. Massachusetts Institute of Technology, Cambridge, MA.
Mazumder, R., 2003. Sediment transport, aqueous bedform stability and morphodynamics under unidirectional current: a brief overview. J. Afr. Earth Sci. 36, 1–14.
McCave, I.N., 1971. Sand waves in the North Sea off the coast of Holland. Mar. Geol. 10, 199–225.
Meyer-Peter, E., Muller, R., 1948. Formulas for bed-load transport. Report on Second Meeting of International Association for Hydraulic Research, p. 39–64.
Morelissen, R., Hulscher, S.J.M.H., Knaapen, M.A.F., Nemeth, A.A., Bijker, R., 2003. Mathematical modelling of sand wave migration and the interaction with pipelines. Coast. Eng. 48 (3), 197–209.
Redding, J.H., 2002. Experimental manipulation of sandwaves to reduce their navigation hazard potential, Jade shipping channel, N. Germany. In: Trentesaux, A., Garlan, T. (Eds.), Proceedings Marine Sandwave Dynamics International Workshop, University of Lille, France.
Rubin, D.M., McCulloch, D.S., 1980. Single and superimposed bedforms: a synthesis of San Francisco Bay and flume observations. Sediment. Geol. 29, 207–231.
Salsman, G.G., Tolbert, W.H., Villars, R.G., 1966. Sand-ridge migration in St. Andrews Bay, Florida. Mar. Geol. 4, 11–19.
Shore Protection Manual, 1984. Shore Protection Manual. US Army Corps of Engineers, Coastal Engineering Research Center, Washington DC.
Simons, D.B., Richardson, E.V., 1961. Forms of bed roughness in alluvial channels. J. Hydraul. Div. 87 (HY3), 87–107.
Sirkin, L., 1995. Eastern Long Island geology with field trip. Book and Tackle Shop, Watch Hill, RI. 220 pp.
Soulsby, R., 1997. Dynamics of Marine Sands. Thomas Telford, London. 249 pp.
Southard, J.B., 1971. Presentation of bed configurations in depth–velocity–size diagrams. J. Sediment. Petrol. 41 (4), 903–915.
Southard, J.B., Boguchwal, L.A., 1990a. Bedform configurations in steady unidirectional water flows. Part 2: synthesis of flume data. J. Sediment. Petrol. 60 (5), 658–679.
Southard, J.B., Boguchwal, L.A., 1990b. Bedform configurations in steady unidirectional water flows. Part 3: effects of temperature and gravity. J. Sediment. Petrol. 60 (5), 680–686.
Stewart, H.B., Jordan, G.F., 1964. Underwater sand ridges on Georges Shoal. In: Miller, R.J. (Ed.), Papers in Marine Geology. Macmillan, New York, pp. 102–114.
Ten Brinke, W.B.M., Wilbers, A.W.E., Wesseling, C., 1999. Dune growth, decay and migration rates during a large-magnitude flood at a sand and mixed sand-gravel bed in the Dutch Rhine river system. Spec. publ. Int. Assoc. Sedimentol. 28, 15–32.
van den Berg, J.H., 1987. Bedform migration and bed-load transport in some rivers and tidal environments. Sedimentology 34, 681–698.
van Dijk, T.A.G.P., Kleinhans, M.G., 2005. Processes controlling the dynamics of compound sand waves in the North Sea, Netherlands. J. Geophys. Res. 110, F04S10.
van Rijn, L.C., 1984a. Sediment transport, part I: bed load transport. J. Hydraul. Eng. 110 (10), 1431–1456.
van Rijn, L.C., 1984b. Sediment transport, part III: bed forms and alluvial roughness. J. Hydraul. Eng. 110 (12), 1733–1754.
Wilbers, A.W.E., Ten Brinke, W.B.M., 2003. The response of subaqueous dunes to floods in sand and gravel bed reaches of the Dutch Rhine. Sedimentology 50, 1013–1034.
Yalin, S.M., 1964. Geometric properties of sand waves. J. Hydraul. Div. 90 (HY5), 105–120.
Yalin, S.M., 1977. Mechanics of Sediment Transport, Second ed. Pergamon Press, Oxford.
Zarillo, G.A., 1982. Stability of bedforms in a tidal environment. Mar. Geol. 48, 337–351.